INSTITUTE OF PHYSICS PUBLISHING MEASUREMENT SCIENCE AND TECHNOLOGY
Meas. Sci. Technol. **12** (2001) R16–R31 www.iop.org/Journals/mt PII: S0957-0233(01)13738-0

REVIEW ARTICLE

Surface voltage and surface photovoltage: history, theory and applications

Dieter K Schroder

Department of Electrical Engineering, Center for Solid State Electronics Research, Arizona State University, Tempe, AZ 85287-5706, USA

Received 3 May 2000, in final form 19 October 2000, accepted for publication 14 December 2000

Abstract
Surface voltage and surface photovoltage measurements have become important semiconductor characterization tools, largely because of the availability of commercial equipment and the contactless nature of the measurements. The range of the basic technique has been expanded through the addition of corona charge. The combination of surface charge and illumination allows surface voltage, surface barrier height, flatband voltage, oxide thickness, oxide charge density, interface trap density, mobile charge density, oxide integrity, minority carrier diffusion length, generation lifetime, recombination lifetime and doping density to be determined. In this review I shall briefly review the history of surface voltage, then discuss the principles of the technique and give some examples and applications.

Keywords: semiconductors, surface voltage, photovoltage, Kelvin probe, lifetime, diffusion length, charge, oxide, oxide thickness

(Some figures in this article are in colour only in the electronic version; see `www.iop.org`)

1. Introduction

Surface voltage (SV) and surface photovoltage (SPV) semiconductor characterization techniques have become powerful methods to determine a number of material/device parameters. The range of the basic technique has been expanded through the addition of corona charge deposited on the sample. The method is particularly attractive because it is usually contactless with the potential measured with a Kelvin probe. Kelvin probes have traditionally been used to measure the sample work function as a function of surface treatment. They were adapted to semiconductor characterization for oxide charge and later, in combination with optical excitation, to minority carrier diffusion length by surface photovoltage. The introduction of commercial equipment led to widespread adoption by the semiconductor industry. When this contactless technique was further expanded by the addition of deposited corona charge, the application expanded further, leading to characterization of surface voltage, surface barrier height, flatband voltage, oxide thickness, oxide leakage current, interface trap density, mobile charge density, oxide integrity, generation lifetime, recombination lifetime and doping density.

After giving a brief history, I shall discuss charging techniques including both chemical rinses and corona charge. This is followed by the theory of charged surfaces and then by some examples.

2. Some history

Bardeen and Brattain first described the SPV technique in 1953 [1]. They characterized the light-induced surface potential variation in Ge samples with a mechanically vibrating reed. In 1955 Garrett and Brattain presented the basic theory of the photo-induced change of the surface potential in a semiconductor when illuminated with light [2]. In the same year, Moss considered diffusion of photo-generated carriers during surface photovoltage measurements [3]. He called it 'photovoltage' and the 'photovoltaic effect'. The name 'surface photovoltage' appears to have been used first by Brattain and Garret in 1956 using continuous illumination [4]. Morrison used a chopped light signal for capacitive detection of the voltage [5]. The application of SPV to determine the minority carrier diffusion length was proposed by Moss in 1955, by Johnson in 1957 [6], by Quilliet and Gosar in 1960 [7]

and by Goodman in 1961 [8]. It was Goodman's SPV approach that led to the first full-scale implementation of the technique in the semiconductor industry at RCA [9]. It was employed during semiconductor production by inserting high diffusion length wafers into critical furnaces and measuring the diffusion length after heating the wafers to characterize the cleanliness of these furnaces. Through this relatively simple, contactless method, they were able to determine cracked furnace tubes, contaminated solid source diffusion sources, metallic contact contamination and other contamination sources.

Instead of dc surface voltage or photovoltage measurements, lifetimes or diffusion lengths can also be extracted from frequency-dependent, charge-based measurements. Nakhmanson was one of the first to introduce frequency-dependent optically induced lifetime measurements [10]. The equivalent circuit concept has proven to be very powerful for the analysis of such measurements. Some of the earliest papers dealing with equivalent circuits are due to Lehovec and Slobodskoy [11] and Hofstein and Warfield [12].

During charge-based measurements, charge is deposited on the wafer and the semiconductor response is measured by one of several techniques, from a corona source or through a chemical rinse. To understand charge-based measurements, it is necessary to understand Kelvin probe measurements, first proposed by Kelvin in 1881 [13]. Kronik and Shapira give an excellent review of such probes and their various applications [14]. A Kelvin probe is usually operated as a vibrating probe with minimization of the external current. The probes in some characterization instruments are not vibrating and we will refer to such probes as surface voltage probes.

The energy band diagram of the probe–air–semiconductor system is analogous to that of an MOS capacitor with the insulator replaced with air. Positive charges, deposited on the semiconductor surface, deplete the surface of the p-type sample. Photons, incident on the sample, generate excess carriers within the space-charge region and in the quasi-neutral bulk region. The electrons within the scr and within a distance of approximately the minority carrier diffusion length from the edge of the scr are collected in the space-charge region and reduce the surface potential barrier. The barrier lowering is similar to a forward-biased junction and the probe detects the difference of the quasi-Fermi levels. For high-level injection, the surface potential vanishes and the probe achieves its maximum potential [15].

3. Surface charging

A crucial component for charge-based measurements is the surface treatment to create the surface space-charge region. Two options are available: treat the surface chemically or deposit corona charge. During chemical treatment, for n-type silicon, the oxide on the sample surface should removed and then the sample should be boiled in H_2O_2 or in water for about 15 min and then rinsed in deionized water (DI) [16]. Alternately, one can soak the sample in $KMnO_4$ for 1–2 min and then rinse in DI water. These treatments produce a stable depletion surface potential barrier. For p-type silicon very little treatment is required. In the case of very low V_{SPV}, etching in buffered HF followed by a DI water rinse is recommended.

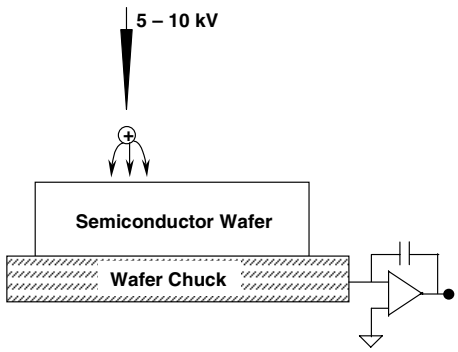

Figure 1. Schematic illustration of a point electrode corona charging method. The deposited charge is precisely measured with the operational amplifier charge meter.

Corona charging is a second method of depositing charge on a surface. It is most commonly used in copying processes using xerographic techniques where the charge is deposited on a photoconductive drum [17]. One of the first uses of deposited charge in the field of semiconductors was by Williams and Willis in the characterization of ZnO in 1968 [18]. Williams and Woods [19] and Weinberg [20] later expanded the approach to the characterization of oxide leakage current and mobile charge drift [21]. The method consists of the deposition of ions on a surface at atmospheric pressure through an electric field applied to a source of ions. The corona source consists of a wire, a series of wires, a single point or multiple points located a few mm or cm above the sample surface [22]. The substrate may be moved during charging or between charging cycles and the sample may be charged uniformly or in well defined areas through a mask arrangement. It is even possible to deposit positive (negative) charge in a given area and surround the area with negative (positive) charge, to act as a guard ring [23]. In contrast to metallic guard rings that always contain a gap between the two electrodes, a corona charge guard ring has zero gap.

A potential of 5000–10 000 V of either polarity is applied to the corona source, as illustrated in figure 1. Ions are generated close to the electrode, where a faint glow may be observed in a darkened room. For a negative source potential, positive ions bombard the source while free electrons are rapidly captured by ambient molecules to form negative ions. For a positive source potential, electrons are attracted to the source and positive ions follow the electric field lines to the substrate. The negative and positive corona ionic species are predominantly CO^{3-} and H_3O^+ (hydrated protons), respectively. The corona source forces a uniform flow of ionized air molecules toward the surface. The very short (approximately 0.1 μm) atmospheric mean free path of the ionized gas ensures collision-dominated ion transport with the molecules retaining very little kinetic energy. The charge is not permanent and can be removed by a water rinse. Typically a few seconds are required to charge an insulating surface to a saturation potential.

One of the advantages for oxide thickness and oxide integrity measurements using corona charge 'gates' rather than conductive gates is the low surface mobility of the 'corona' ions on the sample surface. A charge deposited on the surface of an oxidized wafer, creates an oxide electric field. The oxide will break down at its weakest spot, with the current confined to the breakdown spot, because the surface corona charge does

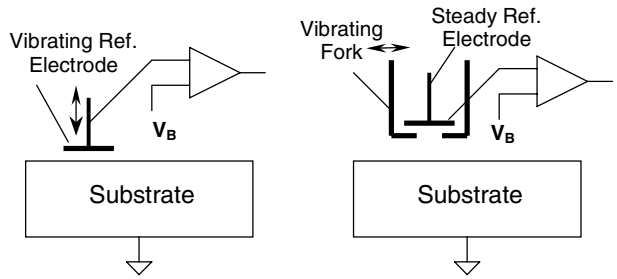

Figure 2. Kelvin probe (left) and Monroe probe (right) for contact potential difference measurements.

not readily drift or diffuse along the surface. By contrast, for a conductive gate with applied gate voltage, the breakdown area may be the same as for the corona charge method, but the current from the entire gate area will be channelled into the weak spot, frequently leading to catastrophic breakdown.

4. Theory

How does a surface voltage or photovoltage come about and how is it measured? A surface voltage is usually the result of a surface or insulator charge or work function difference and it is most commonly detected with a non-contacting probe. The probe is a small plate, 2–4 mm in diameter, held above the sample at a distance of typically 0.1–1 mm. Two types of probe are used, as illustrated in figure 2. In the Kelvin probe, the electrode is vibrated vertically, changing the capacitance between probe and sample. In the Monroe probe, the electrode is fixed and a grounded shutter, mounted in front of the electrode, is vibrated horizontally, thereby modulating the probe to wafer capacitance. The difference in design makes Monroe probes less sensitive to external vibrations so that the measurement setup need not be vibration isolated. Both vibrate at frequencies of typically 500–600 Hz.

The contact potential difference V_{cpd} is determined by measuring the ac current [24]

$$I = V_{cpd}\,\mathrm{d}C/\mathrm{d}t \tag{1}$$

where C is the capacitance between the probe and the sample. The contact potential difference is determined by either calibrating the current versus the bias voltage V_B, or by adjusting V_B until $I = 0$ in which case $V_B = V_{cpd}$. The former method is faster and is used for mapping purposes.

I shall now address the issue of potential and reference potential. The energy or potential band diagram of the probe–air–semiconductor system is shown in figure 3. Potentials are more appropriate than energy because it is the potential that is measured, not the energy. W_M and W_S are the metal and semiconductor work function potentials, i.e., potentials between the vacuum potential E_{vac}/q and the Fermi potential ϕ_F. E_c and E_v are the conduction band and valence band energies and E_c/q and E_v/q their potentials. The potential of the intrinsic energy level in the neutral bulk semiconductor, ϕ, is taken as the reference potential. The *semiconductor* surface potential ϕ_S (ϕ_S is ϕ at $x = 0$) is zero for flatband, positive for depletion and inversion and negative for accumulation.

The potential on the sample surface is the surface voltage V_S. For a bare sample $V_S = \phi_S$, but for an oxidized wafer with charge in or on the oxide, $V_S \neq \phi_S$. The potential measured at the probe is the contact potential difference, also called the contact potential V_{cpd}, which I shall denote as the probe potential V_P from now on. All potentials are measured with respect to the grounded substrate. The probe voltage is the difference in Fermi potential between probe and substrate.

First consider the bare, grounded p-type semiconductor in figure 3 with the metal probe placed a distance t_{air} above the sample. The external nulling voltage V_B ensures zero probe current and zero probe charge. There is no surface charge and W_M and W_S are equal in this example in figure 3(a), leading to the work function difference $W_{MS} = W_M - W_S = 0$. Later we will relax this simplification. The band diagram is very similar to that of an MOS capacitor, with the oxide replaced by air. Next, positive charge of charge density Q (C cm^{-2}) is deposited on the semiconductor surface as in figure 3(b), inducing charge density Q_S in the semiconductor. The dashed lines on the energy band diagram pertain for zero charge and the solid lines for charge density Q, inducing charge only in the semiconductor, not in the nulled probe. Hence, no electric field exists between the sample and the probe making $V_P = V_S = \phi_S$.

The induced semiconductor charge density Q_S, in the absence of an inversion layer, consists of ionized acceptors in the space-charge region (scr)

$$Q = -Q_S = qN_AW \tag{2}$$

where W is the scr width and N_A the acceptor density. To determine the surface voltage, we use the expression for W

$$W = \frac{Q}{qN_A} = \sqrt{\frac{2K_s\varepsilon_0\phi_s}{qN_A}}. \tag{3}$$

Solving for the surface potential ϕ_S gives

$$\phi_s = \frac{Q^2}{2K_s\varepsilon_0qN_A} = \frac{(qN)^2}{2K_s\varepsilon_0qN_A} = 9.07\times10^{-7}\frac{N^2}{K_sN_A} \tag{4}$$

where N is the surface charge atom density (cm^{-2}). As an example, for a Si sample with $N_A = 10^{16}$ cm^{-3}, $K_s = 11.7$, and a surface charge atom density $N = 10^{11}$ cm^{-2}, we find $\phi_S = 0.077$ V.

Many semiconductor samples that are characterized by SV or SPV techniques are oxidized and contain charges and work function differences. To understand the effect of work function differences *and* charge density on surface voltage, we will first consider the simpler and well known MOS capacitor (MOS-C) in figure 4, containing work function difference W_{MS}, positive oxide charge density ρ_{ox} (C cm^{-3}) distributed throughout the oxide, and a positive charge sheet Q_1 (C cm^{-2}) at $x = x_1$. The gate voltage is given by [25]

$$V_G = V_{FB} + V_{ox} + \phi_s \tag{5}$$

where V_{ox} is the potential across the oxide. The flatband voltage is given by

$$V_{FB} = W_{MS} - \frac{x_1}{t_{ox}}\frac{Q_1}{C_{ox}} - \frac{1}{C_{ox}}\int_0^{t_{ox}}\frac{x}{t_{ox}}\rho_{ox}\,\mathrm{d}x \tag{6}$$

where t_{ox} is the oxide thickness.

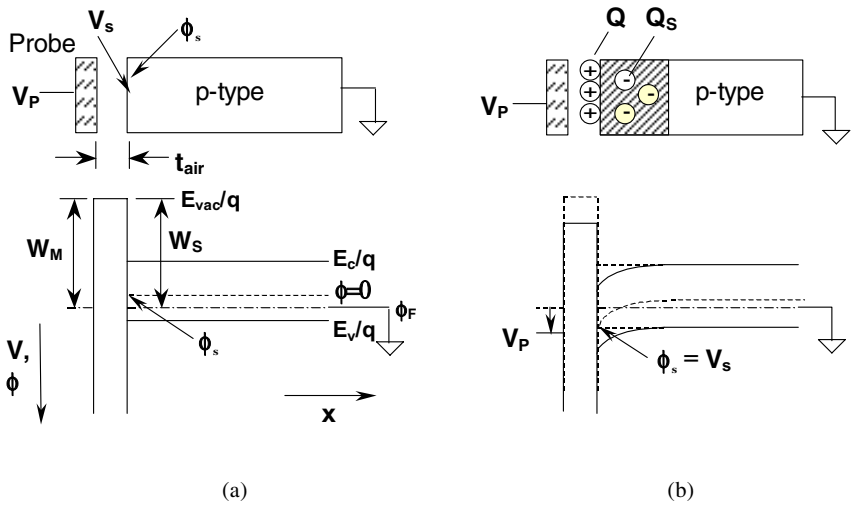

(a) (b)

Figure 3. Cross section and band diagram of a metal–air–semiconductor system with zero work function difference: (a) no surface charge, (b) with surface charge.

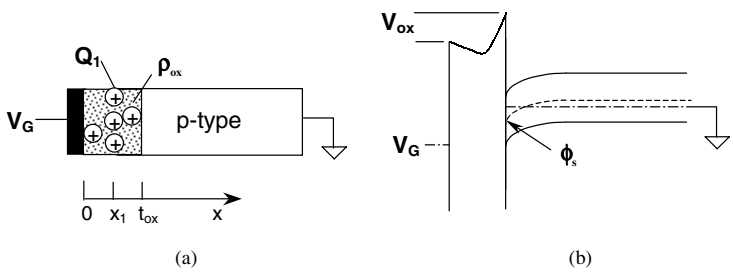

(a) (b)

Figure 4. (a) MOS capacitor cross section showing a charge sheet Q_1 at $x = x_1$ and uniform charge ρ_{ox} throughout the oxide; (b) the corresponding band diagram showing oxide and surface potentials.

Let us now extend this example to a Kelvin probe held above a semiconductor covered with an insulator and a probe–semiconductor work function difference W_{MS} leading to the negative probe potential $V_P = W_{MS}$ in figure 5(a). Next consider oxide charge density ρ_{ox} (C cm^{-3}) and surface charge density Q (C cm^{-2}) as in figure 5(b). These charges induce charge density qN_AW in the semiconductor (indicated by the negative charges) and qn on the probe (indicated by the solid circles, representing electrons). The probe voltage, calculated with the same approach as used for MOS capacitors, is

$$V_P = V_{FB} + V_{air} + V_{ox} + \phi. \tag{7}$$

The flatband voltage in this case is

$$V_{FB} = W_{MS} - \frac{t_{air}}{t_{equ}}\frac{Q}{C_{equ}} - \frac{1}{C_{equ}}\int_{t_{air}}^{t_{equ}} \frac{x}{t_{equ}}\rho_{ox}\,\mathrm{d}x \tag{8}$$

where C_{equ} is the equivalent capacitance and t_{equ} the equivalent thickness given by

$$C_{equ} = \frac{C_{air}C_{ox}}{C_{air}+C_{ox}} = \frac{\varepsilon_0}{t_{equ}} \qquad t_{equ} = t_{air} + t_{ox}/K_{ox}. \tag{9}$$

Equations (7)–(9) show the probe voltage to be due to W_{MS}, Q and ρ_{ox}. A single measurement is unable to distinguish between these three parameters.

Next we will consider the effect of light on the sample. For simplicity, we will use the bare sample in figure 6. Figure 6(a) shows the band diagram with surface charge density Q in the dark and in figure 6(b) the sample is strongly illuminated driving the semiconductor to the flatband condition and the probe potential approaches zero. Hence by measuring the surface voltage without and with light, we obtain the surface potential and hence the charge density from equation (4). To understand how this comes about, we must look at the flatband condition in more detail.

The semiconductor charge density Q_S for a p-type semiconductor in depletion or inversion is

$$Q_S = -\sqrt{2kTK_s\varepsilon_0 n_i}\,F(U_S, K) \tag{10}$$

where F is the normalized surface electric field, defined as [26]

$$F(U_S, K) = [K(\mathrm{e}^{-U_S} + U_S - 1) + K^{-1}(\mathrm{e}^{U_S} - U_S - 1) + K(\mathrm{e}^{U_S} + \mathrm{e}^{-U_S} - 2)\Delta]^{1/2}. \tag{11}$$

In this expression $K = p_0/n_i$ (p_0 is the majority carrier density and n_i the intrinsic carrier density), $U_s = q\phi_s/kT$ is the normalized surface potential, ϕ_s the surface potential and Δ the normalized excess carrier density ($\Delta = \Delta p/p_0$, where $\Delta p = \Delta n$ is the excess carrier density). In the absence of excess carriers, i.e., in equilibrium, the last term in equation (11) vanishes.

F is plotted versus ϕ_s in figure 7 as a function of the normalized excess carrier density, produced by illuminating the device. The electric field is related to the charge density through equation (10). Constant charge implies constant

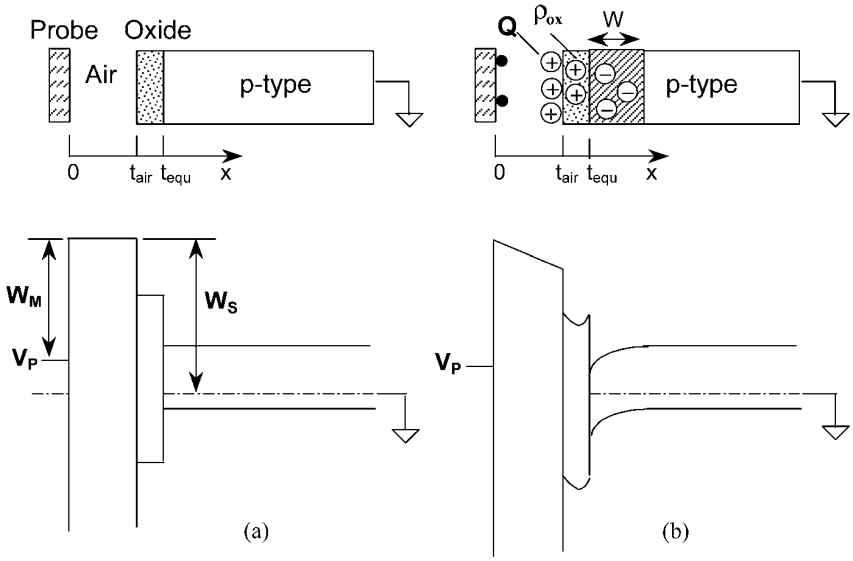

Figure 5. (a) Band diagram for $\phi_{MS} \neq 0$, but zero charges, (b) $\phi_{MS} \neq 0$, $Q \neq 0$ and $\rho_{ox} \neq 0$.

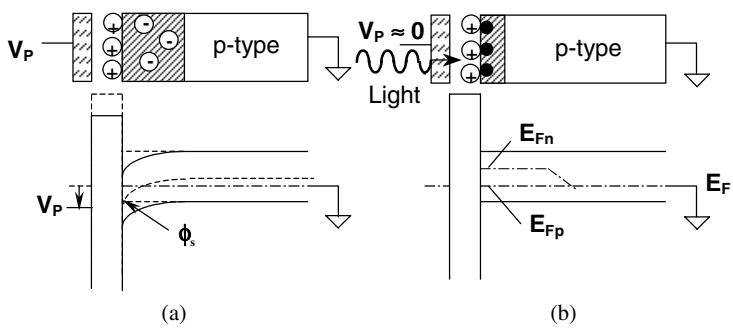

Figure 6. (a) Band diagram with surface charge, (b) band diagram with surface charge and strong illumination. The black circles represent electrons.

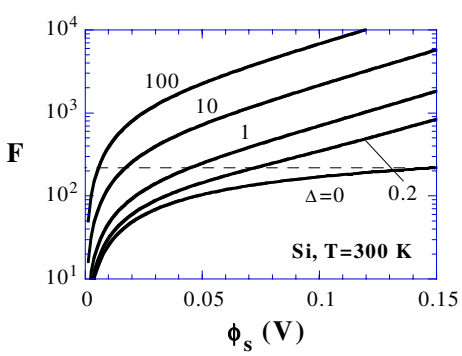

Figure 7. Normalized surface electric field, F, function versus surface potential as a function of normalized excess carrier density or light intensity.

electric field or constant F. Hence as Δn increases, the surface potential decreases, because the locus of the F–ϕ_s plot is along a horizontal line such as the dashed line. It is obvious from figure 7 that the surface potential decreases with increasing light-generated excess carriers. In the limit of intense illumination, $\phi_s \rightarrow 0$ and the semiconductor approaches flatband.

The probe potential is given by

$$V_P = V_{FB} + V_{air} + V_{ox} + \phi_s \tag{12}$$

with V_{ox} given by

$$V_{ox} = Q/C_{ox} = -Q_S/C_{ox} \tag{13}$$

where Q is the surface charge density and Q_S the semiconductor charge density.

The voltages in the dark and under intense illumination ($\phi_S \rightarrow 0$) are given by

$$V_{P,dark} = V_{FB} + V_{air} + Q/C_{ox} + \phi_s$$

$$V_{P,light} = V_{FB} + V_{air} + Q/C_{ox}. \tag{14}$$

The charge density Q remains constant during the measurement, regardless of illumination, and the change in the surface voltage becomes

$$\Delta V_P = V_{P,dark} - V_{P,light} \approx \phi_s. \tag{15}$$

5. Applications

5.1. Minority carrier diffusion length

A major application of SPV is the measurement of minority carrier diffusion length, even though the minority carrier diffusion length plays a negligible role in most integrated circuits (ICs) consisting of MOS devices. Then why measure the minority carrier diffusion length? The reason that minority

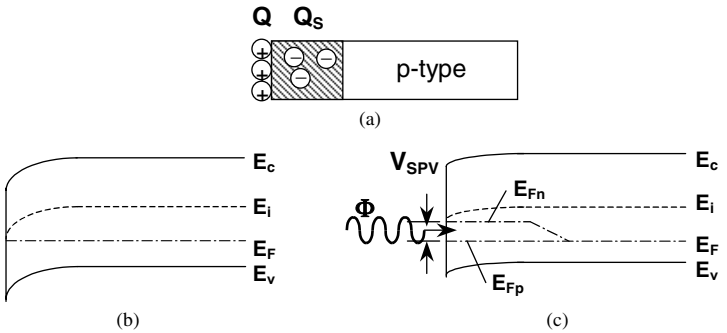

Figure 8. (a) Device cross section showing the surface charge density Q and the semiconductor charge density Q_S, (b) the band diagram in the dark and (c) the illuminated band diagram.

carrier lifetime/diffusion lengths are so commonly measured is that they provide information about the low defect densities consistent with today's integrated circuits. No other technique can detect defect densities as low as 10^9–10^{11} cm^{-3} in a simple, contactless room temperature measurement. In contrast to analytical techniques whose signals are usually proportional to impurity density, lifetime and diffusion length are *inversely* proportional to impurity density. Hence, analytical technique signals *decrease* while lifetime/diffusion length signals *increase* with decreasing impurity density. Further, the availability of commercial, clean room compatible equipment makes these measurements relatively simple. It is for these reasons that the IC community has adopted lifetime/diffusion length measurements as a 'process cleanliness monitor'. The introduction of corona charge has extended the applicability of surface voltage/photovoltage characterization to many other measurements, mentioned above.

Surface photovoltage is an attractive diffusion length characterization technique, because it is nondestructive and contactless, sample preparation is simple (no contacts, junctions, or high temperature processing required), it is a steady-state method and the equipment is commercially available. The concept of surface photovoltage can be understood with the band diagram in figure 8. Surface charge density Q induces an equivalent charge density in the semiconductor, Q_S, with $Q + Q_S = 0$ shown in figure 8(a). The semiconductor charge, in depletion, is provided by the ionized space charge density qN_AW, neglecting electrons and holes in the space-charge region. The band diagram in the dark is shown in figure 8(b). When the sample is illuminated, the Fermi level splits into the quasi-Fermi levels E_{Fn} and E_{Fp} with the surface photovoltage equal to the splitting potential. The band bending is reduced as in figure 8(c).

The sample is assumed to be homogeneous and is of thickness d, as shown in figure 9. One surface is chemically treated to induce a surface space-charge region as described earlier. The wafer can be homogeneous, or it can be in the form of a pn junction or metal–semiconductor junction. We will only treat the homogeneous case here. The surface with the induced scr is uniformly illuminated by monochromatic light of energy higher than the band gap, with the back surface kept in the dark. The light is chopped to enhance the signal/noise ratio using lock-in techniques. The wavelength is varied with a monochromator or a series of filters transmitting selected wavelengths.

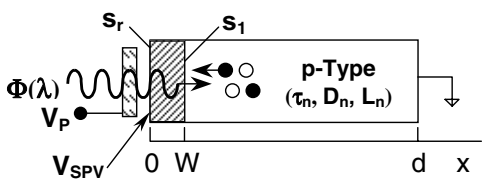

Figure 9. Sample for SPV measurements. The black circles represent electrons and the open circles represent holes.

Electron–hole pairs (ehps) are generated in both the space-charge region (scr) and in the p-substrate by absorbed photons. The ehps generated in the scr are very quickly separated by the electric field with the minority electrons drifting to the surface. Those minority carriers in the quasi-neutral substrate, within approximately a minority carrier diffusion length of the scr edge, diffuse and drift toward the surface, establishing a surface potential or surface photovoltage relative to the grounded back surface. The surface photovoltage is proportional to the excess minority carrier density, $\Delta n(W)$, at the edge of the scr, as described in more detail in appendix A. Light reaching the back surface produces an undesirable SPV signal that can be detected by its large amplitude, by a reversal in signal polarity over the SPV wavelength range or by a signal decrease with increasing illumination at the longer wavelengths.

Equation (A4) in appendix A gives the excess carrier density. In principle, it is possible to extract the diffusion length L_n from that expression for arbitrary W, d and α, the optical absorption coefficient. In practice this is difficult to do and several constraints are usually imposed on the sample to simplify data extraction. The undepleted wafer should be much thicker than the diffusion length and the scr width should be small compared to L_n. The absorption coefficient should be sufficiently low for $\alpha W \ll 1$, but sufficiently high for $\alpha(d - W) \gg 1$. The diameter of the light should be larger than the sample thickness, allowing a one-dimensional analysis and low-level injection (excess carrier density (Δn) is lower than the majority carrier density p_0) should prevail. The assumptions

$$d - W \geqslant 4L_n \qquad W \ll L_n \qquad \alpha W \ll 1$$
$$\alpha(d - W) \gg 1 \qquad \Delta n \ll p_0 \tag{16}$$

allow equation (A4) to be simplified to (see appendix A)

$$\Delta n(W) \approx \frac{(1 - R)\Phi}{(s_1 + D_n/L_n)} \frac{L_n}{(L_n + 1/\alpha)}. \tag{17}$$

As is obvious from the boundary condition in the detailed derivation in appendix A, s_1 is the surface recombination velocity at the edge of the space-charge region, i.e., at $x = W$, not at the surface. The surface recombination velocity at the surface is s_r as illustrated in figure 9.

The excess carrier density at $x = W$ is related to the surface voltage by the 'law of the junction' from pn junction theory

$$\Delta n(W) = n_0(\exp(qV_S/kT) - 1) \approx n_0 qV_S/kT \qquad (18)$$

for $V_S \ll kT/q$. The surface voltage is equal to the probe voltage, giving

$$V_P = \frac{kT}{q}\frac{(1-R)\Phi}{n_0(s_1 + D_n/L_n)}\frac{L_n}{(L_n + 1/\alpha)}. \qquad (19)$$

The dimensions are shown approximately to scale in figure 10.

Optically generated excess carriers diffuse and recombine. Because the electron and hole diffusion coefficients or mobilities differ, a Dember voltage is developed as a result of this mobility difference, given by [27]

$$V_b = \frac{kT}{q}\frac{(b-1)}{(b+1)}\ln\left(1 + \frac{(b+1)\Delta n}{n_0 + bp_0}\right) \qquad (20)$$

where $b = \mu_n/\mu_p$, with μ_n and μ_p the electron and hole mobilities. For p-type Si with $b \approx 3$, $p_0 \gg n_0$ and room temperature, equation (20) becomes

$$V_b = 0.013\ln\left(1 + \frac{4\Delta n}{3p_0}\right) \approx 0.013\frac{4\Delta n}{3p_0}. \qquad (21)$$

With $\Delta n/p_0$ typically 10^{-6}–10^{-4}, $V_b \approx 1.7 \times 10^{-8}$–$1.7 \times 10^{-6}$ V, a voltage that is low compared to the surface photovoltage and is usually neglected.

V_S is proportional to $\Delta n(W)$ for $V_S < 0.5kT/q$. Typical surface photovoltages are in the low millivolt range, ensuring a linear relationship. D_n and L_n are assumed to be constant and over a restricted wavelength range, the reflectivity R can also be considered constant for bare surfaces. The surface recombination velocity s_1 is usually unknown. However, if $\Delta n(W)$ is held constant during the measurement, the surface potential is also constant, and s_1 can be considered reasonably constant. This leaves α and Φ as the only variables.

There are two implementations of the SPV method: (1) constant surface photovoltage and (2) constant photon flux density. In method (1), V_P is held constant, implying $\Delta n(W)$ is also constant. A series of different wavelengths is selected during the measurement with each wavelength providing a different α. The photon flux density Φ is adjusted for each wavelength to hold V_P constant, allowing equation (19) to be written as

$$\Phi = \frac{n_0 V_P(s_1 + D_n/L_n)}{(kT/q)(1-R)}\frac{(L_n + 1/\alpha)}{L_n} = C_1(L_n + 1/\alpha) \qquad (22)$$

where C_1 is a constant.

Then Φ is plotted against $1/\alpha$ for constant V_P. The result is a line whose extrapolated intercept on the negative $1/\alpha$ axis ($\Phi = 0$) is the minority carrier diffusion length L_n, as shown in figure 11(a). The slope of such a plot is C_1, containing the surface recombination velocity s_1. While it is difficult to extract s_1 from the other parameters contained in C_1, it is possible to observe changes in s_1 by comparing SPV plots before and after a surface treatment that changes surface recombination.

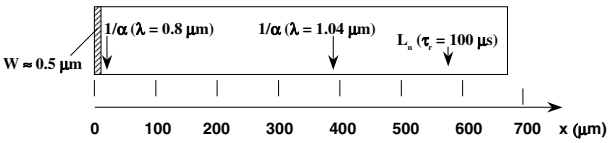

Figure 10. Cross section showing the various lengths for a 675 μm thick p-type wafer.

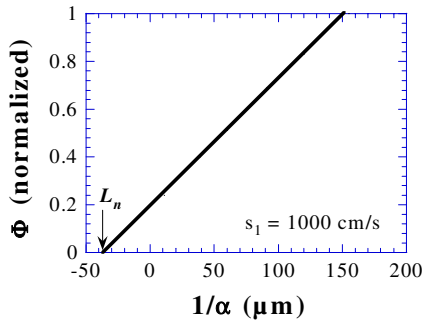

(a)

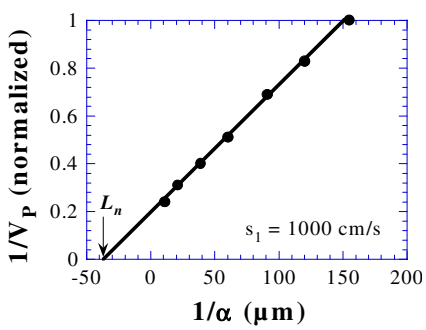

(b)

Figure 11. Normalized SPV plots for (a) constant surface photovoltage (theory) and (b) constant photon flux density (points: data, lines: theory).

For the constant photon flux density implementation, we write equation (19) as

$$\frac{1}{V_P} = \frac{n_0(s_1 + D_n/L_n)}{(kT/q)(1-R)\Phi}\frac{(L_n + 1/\alpha)}{L_n} = C_2(L_n + 1/\alpha) \qquad (23)$$

where C_2 is a constant. A plot of $1/V_P$(normalized) versus $1/\alpha$ gives L_n as illustrated in figure 11(b), where both experimental data and theory are shown. V_P changes during the measurement, hence surface recombination may vary during the measurement. However, the surface photovoltage variation is small and variations in surface recombination velocity are likely to be negligible.

The condition $W \ll L_n$ is generally satisfied for single-crystal Si, but not necessarily for other semiconductors. For example, the diffusion length in GaAs is often only a few microns because radiative recombination dominates. Hence, diffusion length measurements, primarily used for Si to determine recombination centre densities, are less important

in GaAs. In amorphous Si L_n is even shorter. In such a situation the intercept is given by [28]

$$\frac{1}{\alpha} = -L_n\left(1 + \frac{(W/L_n)^2}{2(1 + W/L_n)}\right). \tag{24}$$

For $W \gg L_n$ the $1/\alpha$ intercept is $-W/2$, independent of the diffusion length. For $W = L_n$ the intercept becomes $-5L_n/4$. The scr width can be reduced by shining steady-state light onto the device.

What role does surface recombination play in diffusion length measurements? To answer this question, we have to look at the dependence of the recombination lifetime on bulk and surface recombination. The effective recombination lifetime is [29]

$$\frac{1}{\tau_{eff}} = \frac{1}{\tau_B} + \frac{1}{\tau_S} \tag{25}$$

with the bulk lifetime τ_B and the surface lifetime τ_S given by

$$\tau_B = \frac{\tau_p(n_0 + n_1 + \Delta n) + \tau_n(p_0 + p_1 + \Delta p)}{p_0 + n_0 + \Delta n} \qquad \tau_S = \frac{d}{2s_r} \tag{26}$$

where n_0 and p_0 are the equilibrium carrier densities, Δp the excess carrier density, d the sample thickness, s_r the surface recombination velocity and

$$\tau_p = \frac{1}{\sigma_p v_{th} N_T} \qquad \tau_n = \frac{1}{\sigma_n v_{th} N_T}$$

$$n_1 = n_i\, \mathrm{e}^{(E_T - E_i)/kT} \qquad p_1 = n_i\, \mathrm{e}^{-(E_T - E_i)/kT} \tag{27}$$

with σ_p and σ_n the hole and electron capture cross sections, v_{th} the thermal velocity, N_T the impurity density and E_T the energy level of the impurity. The τ_S term in equation (26) is valid for $s_r < D_n/4d$.

It is obvious that if the effective recombination lifetime depends on surface recombination, so does the effective diffusion length given by

$$L_{n,eff} = \sqrt{D_n \tau_{eff}}. \tag{28}$$

This effect is clearly illustrated in figure 12, where the effective diffusion length is plotted versus the impurity density N_T as a function of surface recombination velocity. This figure clearly illustrates that it becomes increasingly difficult to determine the true diffusion length for low impurity densities except for samples with very low surface recombination velocities. The surface recombination velocity for oxidized/annealed Si is of the order of 100–1000 cm s^{-1}.

Equations (22) and (23) are both proportional to $K(s_1 + D_n/L_n)(L_n + 1/\alpha)$. A plot of either Φ versus $1/\alpha$ or $1/V_P$ versus $1/\alpha$ is linear with an intercept on the negative horizontal $-1/\alpha$ axis of L_n and a slope of $K(s_1 + D_n/L_n)$. While it is difficult to determine s_1 directly, it is possible to observe changes in surface recombination velocity. For example, figure 13 shows two SPV plots of a Si sample before and after surface contamination with copper [30]. As expected, the diffusion length is unchanged, since the Cu has not diffused into the wafer, but surface recombination has changed significantly. This change is consistent with effective recombination lifetime measurements that also show a significant change when the surface is contaminated with copper [31].

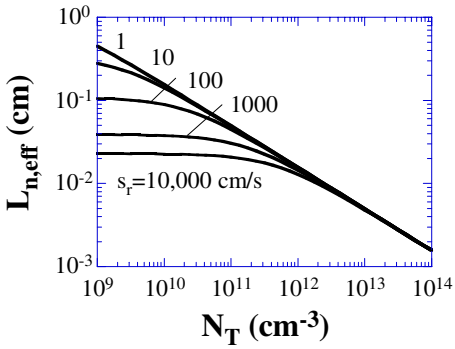

Figure 12. Effective diffusion length $L_{n,eff}$ versus recombination centre density N_T for $E_T = 0.4$ eV, $p_0 = 10^{15}$ cm^{-3}, $\sigma_n = 2 \times 10^{-14}$ cm^2, $\sigma_p = 5 \times 10^{-16}$ cm^2, $\Delta_n/p_0 = 0.01$, $d = 650\ \mu$m, $T = 300$ K and various surface recombination velocities.

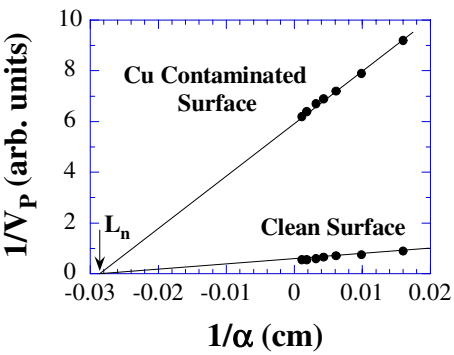

Figure 13. SPV plots of clean and copper-contaminated surfaces. After Lagowski *et al* [30].

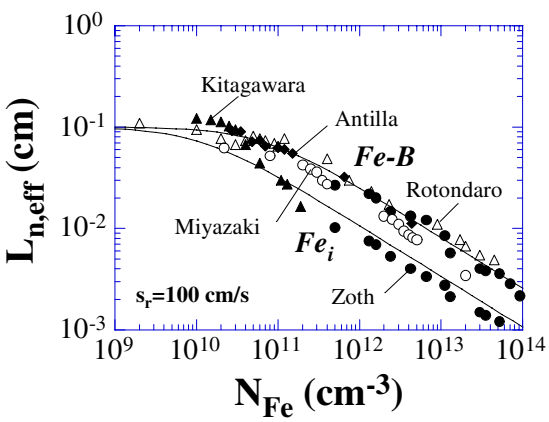

Figure 14. Effective diffusion lengths versus iron density for Fe–B and Fe$_i$. s_r is the surface recombination velocity for the theoretical curves (lines). Data (points) from [35].

5.1.1. Iron in silicon. Iron is one of the most important metallic contaminants in silicon. It usually originates from stainless steel that is extensively used for gas piping, equipment etc. Iron has unique properties in p-type silicon, forming Fe–B pairs in B-doped Si. Chromium, also a constituent of stainless steel, shows similar behaviour [32]. Upon heating at 150–200 °C for a few minutes or illuminating the device (20 W cm^{-2} halogen light source for about 20 s) [33] the Fe–B pairs dissociate into interstitial iron (Fe$_i$) and substitutional boron (B$_s$). The recombination properties of Fe$_i$ differ from

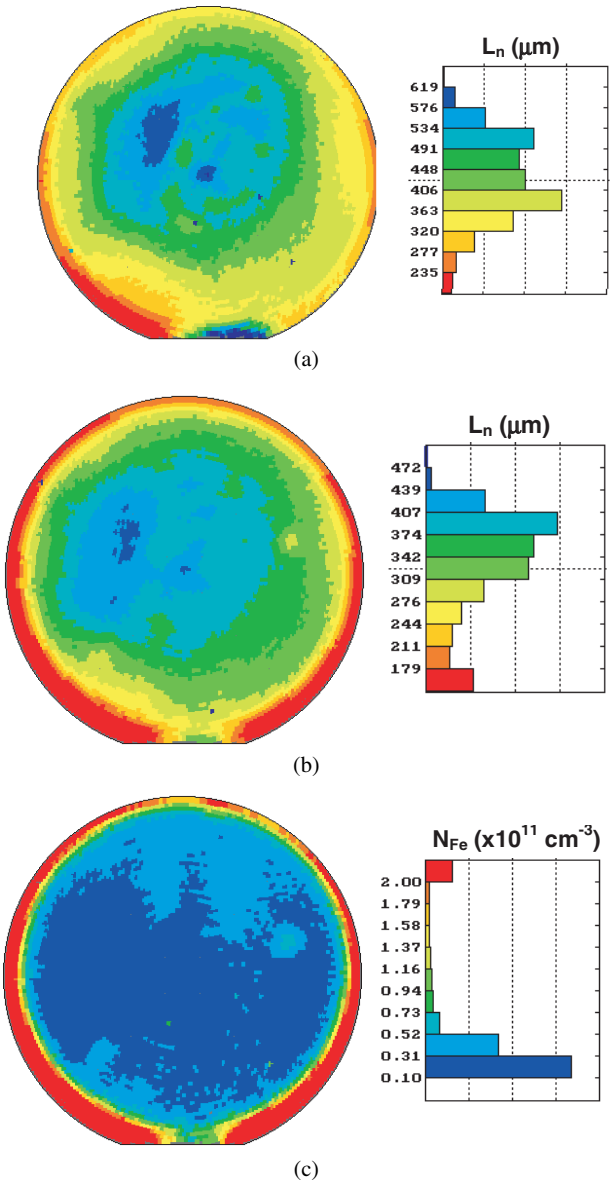

Figure 15. Diffusion length maps (a) before, (b) after Fe–B pair dissociation; (c) iron density map (in units of 10^{11} cm^{-3}). Courtesy of P Edelman and J Lagowski, Semiconductor Diagnostics, Inc.

those of Fe–B. By measuring the diffusion length before (L_{ni}) and after (L_{nf}) Fe–B pair dissociation, the iron density N_{Fe} is obtained from the expression [34]

$$N_{Fe} = 1.05 \times 10^{16}\left(\frac{1}{L_{nf}^2} - \frac{1}{L_{ni}^2}\right) \text{cm}^{-3} \qquad (29)$$

with diffusion lengths in units of μm. The Fe$_i$ and Fe–B diffusion lengths as a function of Fe density are shown in figure 14 [35]. This large difference in diffusion length between Fe$_i$ and Fe–B only pertains at low injection levels and disappears at medium to high injection levels. Maps of diffusion lengths before and after Fe–B pair dissociation and the resultant Fe density are shown in figure 15. Metals rarely pair with impurities in n-type Si, although Cu does form such pairs [36].

5.2. Lifetime

Two types of lifetime are measured in Si wafers: the *recombination* lifetime, τ_r, and the *generation* lifetime, τ_g [29]. As the name implies, the recombination lifetime characterizes the recombination of ehps, while the generation lifetime characterizes the generation of ehps. The recombination lifetime is determined by depositing sufficient charge on an oxidized wafer to invert the semiconductor surface forming a field-induced np junction in a p-type substrate. A brief light pulse forward biases this np junction, injecting excess carriers that subsequently recombine. The resulting time-dependent surface voltage is monitored with a Kelvin probe. This method is very similar to the open-circuit voltage decay technique. τ_r is determined from the equation [37]

$$\tau_r = \frac{kT/q}{\mathrm{d}V_p/\mathrm{d}t}. \qquad (30)$$

The generation lifetime is determined by depositing a charge pulse driving the corona–oxide–semiconductor (COS) device into deep depletion. Electron–hole pairs are subsequently generated and the resulting voltage transient is monitored with a contactless Kelvin probe [23]. These two methods were recently used to characterize both epitaxial films and their substrates [38]. The epitaxial layer is characterized through τ_g measurements, with the thermal carrier generation confined to the charge-induced space-charge region, which is typically of the order of 1 μm below the semiconductor surface. The recombination lifetime, on the other hand, characterizes a depth determined by the minority carrier diffusion length. Figure 16 illustrates corona-induced generation and recombination lifetime measurements of n-epitaxial layers on n-substrates. Figure 16(a) shows the results for both 'good' layer and 'good' substrate with $\tau_g \approx 4$ ms and $\tau_r \approx 300$ μs. Figure 16(b) shows a 'good' epitaxial layer ($\tau_g \approx 3$ ms), but the substrate is contaminated, reducing the recombination lifetime to about 50 μs. While recombination lifetime measurements can be made without corona charge, using conventional surface photovoltage or photoconductance decay measurements, contactless generation lifetime measurements require corona charge.

5.3. Charge

The surface voltage dependence on surface charge lends itself to measurements of charge in the insulator on a semiconductor wafer or charge on the wafer. This charge can be oxide charge, interface trapped charge plasma damage charge, or other charge. Let us illustrate this by considering the mobile charge density Q_m in an oxidized wafer [39]. Such mobile charge in silicon technology is most commonly sodium, originating from such sources as humans, chemicals, equipment etc. Other possible mobile charges are potassium, associated with chemical polishing compounds, and lithium, which can originate from pump oils.

One way to measure such a mobile charge is to combine SV measurements with corona charge techniques by depositing corona charge on an oxidized semiconductor surface. First deposit positive corona charge, then heat the wafer to a moderate temperature of around 200 °C for a few

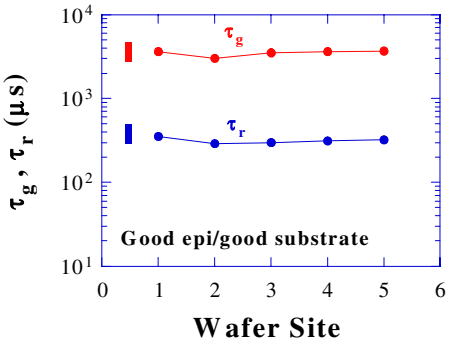

(a)

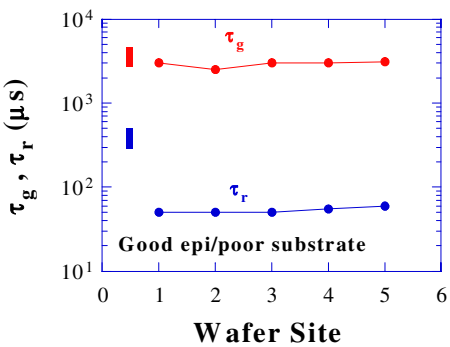

(b)

Figure 16. Corona charge-induced generation and recombination data for (a) good epitaxial layer and substrate, and (b) good epitaxial layer and poor substrate. Data after [38].

minutes, driving the mobile charge to the oxide–semiconductor interface. Cool the sample and determine the flatband voltage V_{FB1}. Next repeat the procedure with a negative corona charge and drive the mobile charge to the oxide–air interface determining V_{FB2}. From equation (8), Q_m is then determined by the flatband voltage difference $\Delta V_{FB} = V_{FB2} - V_{FB1}$ through the relation

$$Q_m = C_{ox}\Delta V_{FB}. \tag{31}$$

Unless the oxide is heavily contaminated, the flatband voltage difference ΔV_{FB} is likely to be very small for today's thin gate oxides.

The sensitivity of the measurement can be enhanced by decreasing the oxide capacitance through thicker oxides, but that is inconsistent with today's thin gate oxides. The problem is illustrated in equation (6). The flatband voltage due to oxide charge density ρ_{ox} alone is $V_{FB} = -\rho_{ox}t_{ox}^2/2K_{ox}\varepsilon_0$. For a charge density of $\rho_{ox}t_{ox}/q = 10^{10}$ cm^{-2}, we find $V_{FB} = -2.3 \times 10^3 t_{ox}$. For example, for $t_{ox} = 10$ nm, $V_{FB} = -2.3$ mV, illustrating that voltage measurements become impractical for thin oxides. A solution to this problem is to take an oxidized wafer and measure the surface potential. We showed earlier that the surface potential can be obtained by surface voltage measurements without and with intense light. Then deposit corona charge until the surface potential becomes zero. The deposited corona charge is then equal in magnitude but opposite in sign to the original oxide charge [40]. The accuracy and precision of this charge-based measurement is identical for thin and thick oxides.

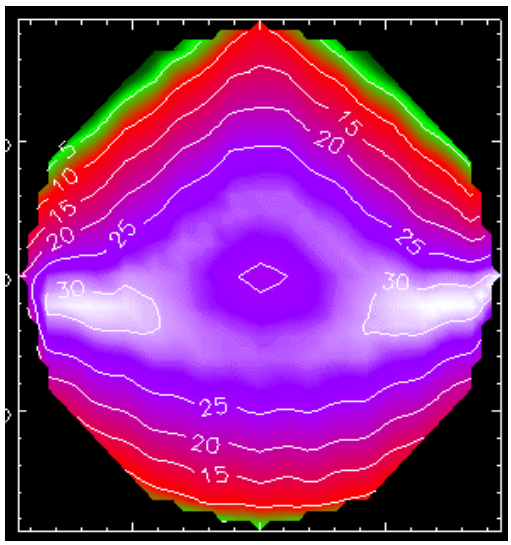

(a)

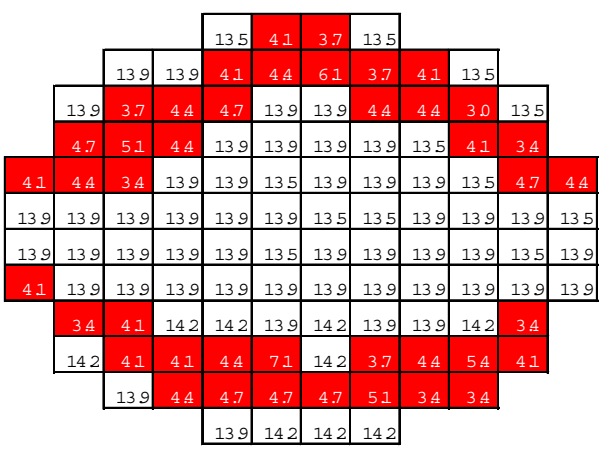

(b)

Figure 17. Plasma damage contour maps measured by (a) corona charge and (b) MOSFET antenna structures. Courtesy of S Weinzierl, KLA-Tencor.

Other charges that have been determined with SV measurements are plasma-induced charge and damage [41]. A map of plasma charge density is shown in figure 17. Another interesting application is the study of hydrogen-stabilized silicon surfaces. Here Si surfaces were exposed to two hydrogen treatments: annealing in hydrogen or immersing in HF [41]. Hydrogen-annealed surfaces were more stable, determined by measuring the surface barrier as a function of time. The measurement of oxide charge in buried oxides of silicon-on-insulator materials is also feasible [42].

5.4. Oxide thickness

Corona charge density Q is deposited on the oxidized wafer and the surface voltage in the dark and under intense light are measured [43]. According to equation (15) this gives the surface potential ϕ_S, which is then plotted as a function of deposited charge density as shown in figure 18 [44]. When the

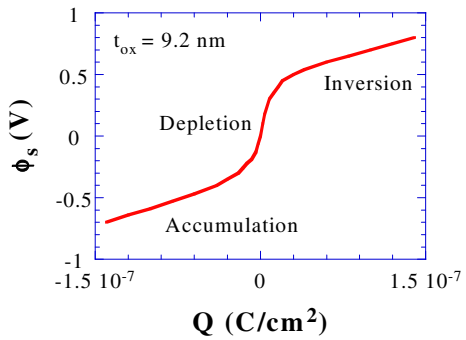

Figure 18. Surface potential versus charge showing the various regions of the device. $t_{ox} = 9.2$ nm. After Roy *et al* [43].

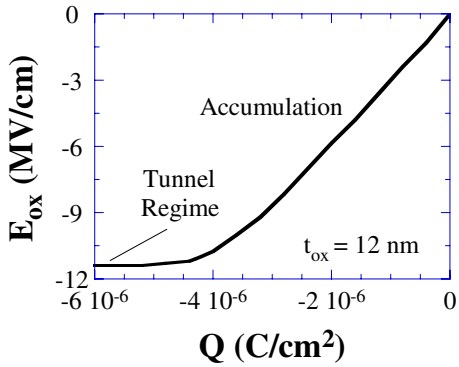

Figure 19. Oxide electric field versus surface charge for an oxidized Si wafer. $t_{ox} = 12$ nm. After Roy *et al* [43].

device is biased into accumulation or inversion, the oxide thickness is given by

$$C_{ox} = \frac{\mathrm{d}Q}{\mathrm{d}\phi_s} \qquad t_{ox} = \frac{K_{ox}\varepsilon_0}{C_{ox}}. \tag{32}$$

This method is not subject to the poly-Si gate depletion effects that affect conventional MOS-C measurements [45]. It is also not affected by probe punchthrough and is relatively insensitive to oxide pinhole leakage currents. Repeatability of 0.01 nm has been demonstrated for 1.8 nm thick oxides [40].

5.5. Oxide leakage current

To determine oxide leakage current, usually known as gate current in MOS devices, corona charge is deposited on the surface of an oxidized wafer and the surface voltage is measured as a function of time. The device is biased into accumulation or inversion and the oxide leakage current is related to the voltage through the relationship [46]

$$I_{leak} = C_{ox}\frac{\mathrm{d}V_P}{\mathrm{d}t} \Rightarrow V_P(t) = \frac{I_{leak}}{C_{ox}}t. \tag{33}$$

When the charge density is too high, the charge leaks very rapidly through the oxide by Fowler–Nordheim or direct tunnelling and the surface voltage is clamped.

The deposited charge density is related to the oxide electric field E_{ox} through the relationship

$$Q = K_{ox}\varepsilon_0 E_{ox} = 3.45 \times 10^{-13} E_{ox} \tag{34}$$

for SiO_2. Silicon dioxide breaks down at electric fields of 10–14 MV cm^{-1}. For $E_{ox} = 12$ MV cm^{-1}, we find the charge to be 4.1×10^{-6} C cm^{-2}. Figure 19 is a plot of E_{ox} versus Q, clearly showing the electric field saturation at a charge density of around 4.4×10^{-6} C cm^{-2}.

6. Frequency-dependent surface photovoltage

Most SPV measurements are made under dc conditions. It may be that the incident light is chopped at a moderate frequency (typically 500–600 Hz) for signal/noise enhancement through lock-in techniques. However, there is information to be gained by using ac-modulated incident light. For example, using frequency-modulated light as the excitation source eliminates the need to vibrate the Kelvin probe. The requirements on the back contact can also be relaxed with a suitable capacitive contact. As shown in appendix B, under such conditions, the frequency-dependent minority carrier diffusion length becomes

$$L_n(\omega) = \frac{L_{n0}}{\sqrt{1 + \mathrm{j}\omega\tau_r}} \tag{35}$$

with L_{n0} the low-frequency value. The surface photovoltage is measured versus the sinusoidally modulated input frequency. The SPV equation becomes

$$V_P(\omega) = \frac{kT}{q}\frac{(1-R)\Phi}{n_0(s_1 + D_n/L_n(\omega))}\frac{L_n(\omega)}{(L_n(\omega) + 1/\alpha)} \tag{36}$$

with the frequency-dependent diffusion length $L_n(\omega)$ given by equation (35).

Nakhmanson originally put forth the theory for frequency-dependent SPV measurements [10]. It was later implemented by Munakata *et al* who proposed [47] and later implemented it with a flying spot scanner incorporating both blue and infrared light sources [48]. The blue light, absorbed near the surface, mainly characterizes the semiconductor near the surface, while the infrared light probes deeper into the wafer. By scanning the light beam, wafer maps can be generated in a few minutes. The surface photovoltage depends on the semiconductor band bending, which depends on the surface charge density. Hence ac SPV measurements lend themselves to surface charge density measurements [49].

In another version of ac SPV, the semiconductor surface is depleted/inverted by chemically induced surface charges and a sinusoidally modulated, low-intensity light generates excess carriers. The carrier lifetime is determined from the ratio of the real and imaginary SPV signals. Short-wavelength light ($\lambda = 0.4$ μm) with high absorption coefficient ensures carrier generation near the surface. Hence, the measured lifetime is primarily determined by the oxide–semiconductor interface, i.e., surface recombination, and is sometimes termed the 'surface lifetime' [50].

In another commercial version, an oxidized wafer is biased into inversion with pulsed light incident on the sample. Optically generated minority carriers add to the inversion charge, reducing the surface potential and space-charge region width. The measured current I_{signal} contains the relevant parameters [51]. The slope of the I_{signal}/Φ versus Φ plot gives the surface lifetime. The signal also contains the substrate doping density or resistivity, leading to contactless resistivity

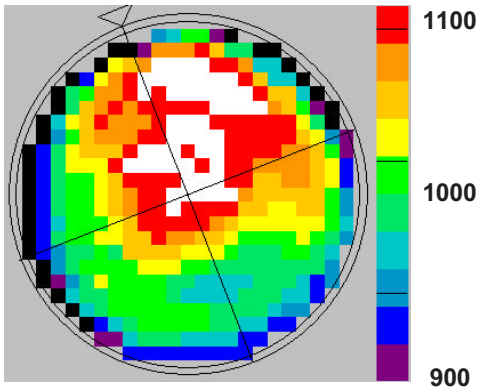

(a)

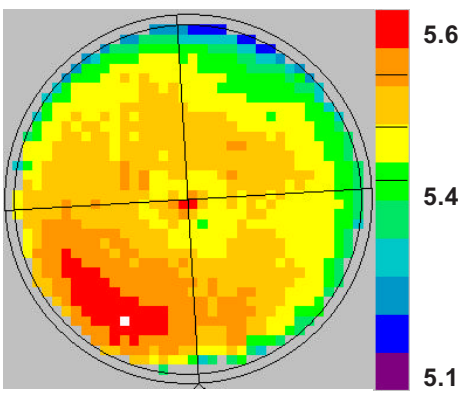

(b)

Figure 20. Resistivity maps of epitaxial layers determined by ac SV measurements. The values are in ohm cm. The black peripheral ring in (a) is low resistivity (<5.1 ohm cm) due to outdiffusion from the heavily doped substrate. Courtesy of M C Nguyen, Epitech.

measurements [52]. Resistivity maps of epitaxial layers are shown in figure 20 [53]. Figure 20(a) shows the resistivity of a high-resistivity n-epitaxial layer grown on a heavily doped n^+ (arsenic) substrate with the substrate back surface sealed by a deposited oxide to prevent outdiffusion. Figure 20(b) shows what happens when the substrate back surface is not sealed and auto-doping causes the epitaxial layer to be contaminated with a resultant low resistivity.

7. Experimental considerations

In SPV plots, the photon flux density or inverse surface photovoltage is plotted against the inverse absorption coefficient. It is not the absorption coefficient, however, but the wavelength that is varied during the measurement. An accurate wavelength-absorption coefficient relationship is, therefore, very important for these measurements. Any error in that relationship leads to incorrect diffusion lengths. Various equations have been proposed. A fit to recent α–λ data for silicon is given by [54]

$$\alpha = \left(\frac{83.15}{\lambda} - 74.87\right)^2 \tag{37}$$

with the wavelength λ in μm and the absorption coefficient α in cm^{-1} units, valid for the 0.7 to 1.1μm wavelength range typically used for Si SPV measurements.

The reflectance R in SPV equations is usually considered to be constant. However, there is a weak wavelength dependence for bare Si, given by [55]

$$R = 0.3214 + \frac{0.035\,65}{\lambda} - \frac{0.031\,49}{\lambda^2} \tag{38}$$

for $0.7 < \lambda < 1.05$ μm with λ in μm.

8. Cautions

8.1. Wafer thickness

All diffusion length measuring techniques yield the true diffusion length only for samples thicker than $3L_n$. *Effective* diffusion lengths are determined for thinner samples [56]. But for samples thinner than L_n, it is difficult to extract the correct diffusion length [57]. This is of particular concern for thin epitaxial layers on heavily doped substrates. Recent lifetime measurements on epitaxial layers have shown this to be true [58]. The effective lifetime, being a combination of epitaxial and substrate lifetimes, was mainly governed by the low-lifetime substrate, determined by measuring the lifetime before and after epitaxial film etching.

To see the effect of diffusion length and sample thickness on SPV plots, Φ and $1/\Phi$ are plotted against $1/\alpha$ as a function of L_n using the exact equation (A4) for Si in figure 21. Figure 21(a) shows a good linear fit to the calculated data for $(3\text{–}4)L_n \leqslant d$ as expected, but there is poor linearity for longer diffusion lengths and the simple analysis of equation (22) is no longer valid. For $x = 0$, $d \ll L_n$, and $\alpha d \gg 1$, equation (A4) becomes

$$\Delta n(0) = \frac{(1-R)\Phi\alpha\tau}{(\alpha^2 L_n^2 - 1)}\left(\frac{s_2\alpha d + \alpha D - Dd/L_n^2 - s_2}{s_1 s_2 d/D + Dd/L_n^2 + s_1 + s_2}\right)$$
$$\approx \frac{(1-R)\Phi}{(1-1/\alpha^2 L_n^2)}\left(\frac{d - 1/\alpha}{s_1 d + D}\right) \tag{39}$$

valid for high s_2. A $1/\Phi$ versus $1/\alpha$ plot, according to

$$\frac{1}{\Phi} \approx \frac{(1-R)}{\Delta n(0)(1-1/\alpha^2 L_n^2)}\frac{(d - 1/\alpha)}{(s_1 d + D)} \tag{40}$$

has a $1/\alpha$ intercept of d at $1/\Phi$ provided $(\alpha L_n)^2 \gg 1$. This is illustrated in figure 21(b) where the low-$1/\alpha$ extrapolated intercept is close to the wafer thickness $d = 500$ μm, as predicted by equation (40), but only for high L_n. The second extrapolated $1/\alpha$ intercept gives neither L_n nor d. It is obvious from these figures that the diffusion length cannot be reliably determined with the simple SPV equations when it exceeds the sample thickness.

8.2. Optical beam diameter

The optical beam diameter has an influence on the measured diffusion length. A detailed study has shown that for long diffusion length material, a probe diameter, d_{probe}, equal to the light beam diameter, d_{light}, yields diffusion lengths substantially lower than the true diffusion length [59]. For example, for a 6 mm diameter probe and a 6 mm diameter

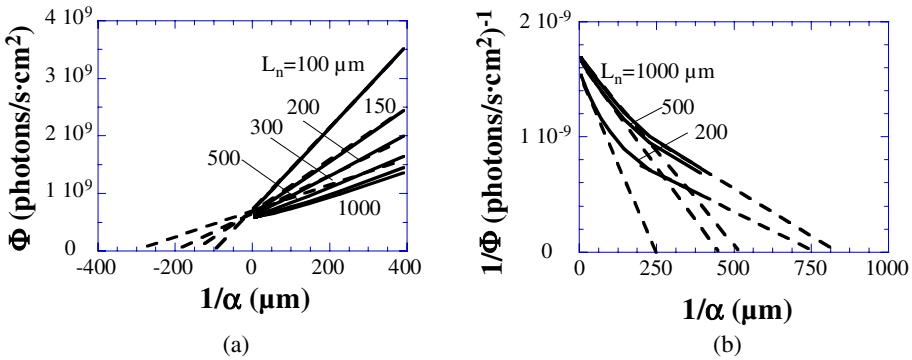

Figure 21. Constant voltage SPV plots of exact equation and approximation. (a) Φ versus $1/\alpha$ and (b) $1/\Phi$ versus $1/\alpha$. The solid lines are the exact calculations (equation (A4)) and the dashed lines are the extrapolations. $s_1 = 10^4$ cm s^{-1}, $s_2 = 10^4$ cm s^{-1}, $D_n = 30$ cm^2 s^{-1}, $V_P = 10$ mV, $R = 0.3$, $n_0 = 10^5$ cm^{-3} and $d = 500$ μm.

light beam, a 1500 μm diffusion length would be measured as 675 μm and a 750 μm diffusion length would be measured as 525 μm. For $d_{light} - d_{probe} \approx 2L_{n,real}$, the error becomes insignificant [60].

8.3. Reflectivity

The light intensity transmitted into the sample depends on the reflectivity. The reflectivity for bare wafers is reasonably constant with wavelength. However, for oxidized wafers R depends on insulator film thickness and on wavelength. Hence the effective photon flux density, $\Phi_{eff} = (1 - R)\Phi$, must be known for correct interpretation of SPV diffusion length measurements.

8.4. Temperature

Temperature causes α to change because the semiconductor band gap is temperature dependent. Higher measurement temperature leads to lower band gap and higher α. Hence, if the measurement temperature is higher than the usual room temperature, the value of L_n extracted from such SPV measurements will be too high due to the temperature dependence of the absorption coefficient.

8.5. Trapping

Trapping centres in the semiconductor capture carriers and then release them back to the band from which they were captured. Excess ehps are generated by light. Instead of recombining directly, some electrons are temporarily captured or trapped. They are subsequently re-emitted into the conduction band, and finally recombine with the holes. Clearly the electrons 'live' longer in this case by the length of time that they are trapped, and diffusion length measurements give erroneously high values.

Trapping is detected in SPV measurements, for example, by a diffusion length dependence on photon flux density [61] and can be much reduced by illuminating the sample with a steady-state background light. The light continually creates ehps, keeping the traps filled, and additional ehps will recombine with reduced trapping.

9. Summary

Surface voltage and surface photovoltage measurements are the topic of this review. After a brief history, tracing the basic technique to 1953, the theory of these techniques is developed. In order for a surface voltage to exist, it is necessary to deposit charge on the sample by some means. This is most commonly done by rinsing the sample in certain solutions or depositing corona charge on it. Rinsing is usually done on bare samples and corona charge is deposited on samples covered by insulators. The use of these contactless measurement techniques has broadened from initial application of minority carrier diffusion length measurements to a wide variety of semiconductor characterization, including surface voltage, surface barrier height, flatband voltage, oxide thickness, oxide charge density, interface trap density, mobile charge density, oxide integrity, generation lifetime, recombination lifetime and doping density. It is likely that this range of application will broaden further. As with all characterization techniques, there are limitations and some of these are also discussed. I have chosen to give detailed derivations of the necessary concepts, including liberal use of band diagrams, because this aspect of the technique is rarely discussed in the published literature.

Acknowledgments

The research leading to this paper was partially funded by the Silicon Wafer Engineering and Defect Science Consortium (SiWEDS) (Intel, Komatsu Electronic Metals, MEMC Electronic Materials, Mitsubishi Silicon, Okmetic, Nippon Steel, SEH America, Sumitomo Sitix Silicon, Texas Instruments, and Wacker Siltronic Corp.). I wish to thank them for their support. I also wish to thank the anonymous reviewer for a thorough review and for thoughtful comments, allowing the manuscript to be improved.

Appendix A. DC excitation

We first consider the p-type semiconductor of figure A1(a). It is a wafer of thickness d, reflectivity R, minority carrier lifetime τ, minority carrier diffusion coefficient D, minority carrier diffusion length L and surface recombination velocities s_1 and s_2 at the front and back surfaces. Monochromatic light of

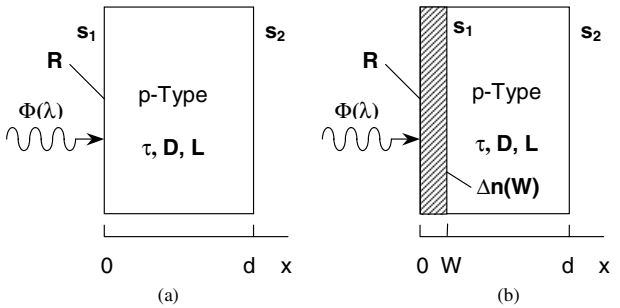

Figure A1. Homogeneous p-type sample geometry with optical excitation: (a) neutral, (b) with surface-induced space-charge region.

photon flux density Φ, wavelength λ and absorption coefficient α is incident on one side of this wafer. We assume that carriers generated by absorbed photons diffuse in the x-direction and that the wafer has infinite extent in the y–z-plane, allowing the neglect of edge effects. The steady state, small-signal excess minority carrier density $\Delta n(x)$ is obtained from a solution of the one-dimensional continuity equation

$$D\frac{\mathrm{d}^2\Delta n(x)}{\mathrm{d}x^2} - \frac{\Delta n(x)}{\tau} + G(x) = 0 \qquad \text{(A1)}$$

subject to the boundary conditions

$$x = 0\text{:}\ \frac{\mathrm{d}\Delta n(x)}{\mathrm{d}x}_{x=0} = s_1\frac{\Delta n(0)}{D}$$

and

$$x = \mathrm{d}\text{:}\ \frac{\mathrm{d}\Delta n(x)}{\mathrm{d}x}_{x=\mathrm{d}} = -s_2\frac{\Delta n(\mathrm{d})}{D}. \qquad \text{(A2)}$$

The electric field in the semiconductor sample is low and is neglected for simplicity. The generation rate is given by

$$G(x,\lambda) = \Phi(\lambda)\alpha(\lambda)[1 - R(\lambda)]\exp(-\alpha(\lambda)x). \qquad \text{(A3)}$$

An implicit assumption in this expression is that each *absorbed* photon generates one ehp. This is usually a good assumption for semiconductors.

The solution to equation (A1) using (A2) and (A3) is [62]

$$\begin{aligned}\Delta n(x) = \frac{(1-R)\Phi\alpha\tau}{(\alpha^2L^2-1)}\Bigg\{\Bigg[K_1\sinh\left(\frac{d-x}{L}\right)\\ +K_2\cosh\left(\frac{d-x}{L}\right)+\mathrm{e}^{-\alpha d}\Bigg[K_3\sinh\left(\frac{x}{L}\right)\\ +K_4\cosh\left(\frac{x}{L}\right)\Bigg]\Bigg]\Bigg[\left(\frac{s_1s_2L}{D}+\frac{D}{L}\right)\sinh\left(\frac{d}{L}\right)\\ +(s_1+s_2)\cosh\left(\frac{d}{L}\right)\Bigg]^{-1} - \mathrm{e}^{-\alpha x}\Bigg\}\end{aligned} \qquad \text{(A4)}$$

where

$$K_1 = \frac{s_1s_2L}{D} + s_2\alpha L \qquad K_2 = s_1 + \alpha D$$

$$K_3 = \frac{s_1s_2L}{D} - s_1\alpha L \qquad K_4 = s_2 - \alpha D.$$

For SPV measurements, a surface charge induced space-charge region of width W exists as shown in figure A1(b). The light generates excess carriers and it is well known from pn junction theory (law of the junction) that the excess carrier density at the scr edge is related to the resulting surface voltage V_S through the relation [25]

$$\Delta n(W) = n_0(\exp(qV_S/kT) - 1) \approx n_0qV_S/kT \qquad \text{(A5)}$$

where n_0 is the equilibrium minority carrier density. The approximation in equation (A5) holds for $V_S \ll kT/q$.

To determine the surface voltage, we need an expression for $\Delta n(W)$. For $x = W$, equation (A4) becomes

$$\begin{aligned}\Delta n(W) = A\Bigg\{\Bigg[K_1\sinh\left(\frac{d-W}{L}\right)+K_2\cosh\left(\frac{d-W}{L}\right)\\ +\mathrm{e}^{-\alpha d}\Bigg[K_3\sinh\left(\frac{W}{L}\right)+K_4\cosh\left(\frac{W}{L}\right)\Bigg]\Bigg]\\ \times\Bigg[\left(\frac{s_1s_2L}{D}+\frac{D}{L}\right)\sinh\left(\frac{d}{L}\right)+(s_1+s_2)\cosh\left(\frac{d}{L}\right)\Bigg]^{-1}\\ -\mathrm{e}^{-\alpha W}\Bigg\}\end{aligned} \qquad \text{(A6)}$$

with $A = (1-R)\Phi\alpha\tau/(\alpha^2L^2-1)$. Let us now examine the various assumptions that are made for the simplified equation usually used to analyse SPV data. The space-charge region width W is usually much smaller than the wafer thickness d, hence $d - W \approx d$. Assumption (i): $d - W \gg L$, i.e., the wafer is much thicker than the minority carrier diffusion length. This allows equation (A6) to be written as

$$\begin{aligned}\Delta n(W) = A\Bigg\{\Bigg[(K_1+K_2)\Bigg[\cosh\left(\frac{W}{L}\right)-\sinh\left(\frac{W}{L}\right)\Bigg]\\ +\mathrm{e}^{-\alpha d}\Bigg[K_3\sinh\left(\frac{W}{L}\right)+K_4\cosh\left(\frac{W}{L}\right)\Bigg]\Big/\cosh(d/L)\Bigg]\\ \times\left[\frac{s_1s_2L}{D}+\frac{D}{L}+s_1+s_2\right]^{-1} - \mathrm{e}^{-\alpha W}\Bigg\}.\end{aligned} \qquad \text{(A7)}$$

For $W \ll L$ and $\alpha(d - W) \approx \alpha d \gg 1$, we have

$$\begin{aligned}\Delta n(W) = \frac{(1-R)\Phi\alpha\tau}{(\alpha^2L^2-1)}\Bigg\{\Bigg((K_1+K_2)\Bigg[1-\frac{W}{L}\Bigg]\Bigg)\\ \times\left(\frac{s_1s_2L}{D}+\frac{D}{L}+s_1+s_2\right)^{-1} - \mathrm{e}^{-\alpha W}\Bigg\}.\end{aligned} \qquad \text{(A8)}$$

The assumption $\alpha W \ll 1$ leads to

$$\begin{aligned}\Delta n(W) &= \frac{(1-R)\Phi\alpha L}{(\alpha^2L^2-1)}\Bigg\{\Bigg[\left(s_2+\frac{D}{L}\right)(\alpha L-1)\left(1+\frac{s_1W}{D}\right)\Bigg]\\ &\quad\times\left[s_2s_1+\frac{D}{L}\left(\frac{D}{L}+s_1+s_2\right)\right]^{-1}\Bigg\}\\ &= \frac{(1-R)\Phi\alpha L}{(\alpha L+1)}\Bigg\{\Bigg[\left(1+\frac{D}{s_2L}\right)\left(1+\frac{s_1W}{D}\right)\Bigg]\\ &\quad\times\left[s_1+\frac{D}{L}\left(1+\frac{D}{s_2L}+\frac{s_1}{s_2}\right)\right]^{-1}\Bigg\}.\end{aligned} \qquad \text{(A9)}$$

If we assume the back contact to have very high surface recombination, i.e., $s_2 \to \infty$, equation (A9) becomes

$$\Delta n(W) = \frac{(1-R)\Phi\alpha L}{(\alpha L+1)}\left(\frac{1+s_1W/D}{s_1+D/L}\right). \qquad \text{(A10)}$$

The term s_1W/D is usually $\ll 1$, leading to

$$\Delta n(W) = \frac{(1-R)\Phi}{(s_1+D/L)}\frac{\alpha L}{(1+\alpha L)} \qquad \text{(A11)}$$

which is the desired result.

Appendix B. Sinusoidal excitation

In some measurement techniques, a phase shift between the optical excitation source and the detected parameter is measured. For a sinusoidally varying generation rate,

$$G(x,t) = (G_0 + G_1 e^{j\omega t})\, e^{-\alpha x} = (\Phi_0 + \Phi_1 e^{j\omega t})\alpha(1-R)\, e^{-\alpha x} \tag{B1}$$

the fundamental component of the variation of the excess minority carrier density $\Delta n_1(x)\exp(j\omega t)$ is determined from the equation

$$D\frac{d^2\Delta n_1(x)}{dx^2} - \frac{\Delta n_1(x)}{\tau} + G_1 e^{-\alpha x} = j\omega\Delta n_1(x). \tag{B2}$$

The solution to this equation, subject to the same boundary conditions as equation (A1), is similar to equation (A4), with L replaced by $L/(1+j\omega\tau)^{1/2}$, the frequency-dependent diffusion length. The sinusoidally varying light is obtained by modulating a semiconductor laser. The time varying surface photovoltage and phase are measured as a function of frequency.

References

[1] Brattain W H and Bardeen J 1953 Surface properties of germanium *Bell Syst. Tech. J.* **32** 1–41

[2] Garrett C G B and Brattain W H 1955 Physical theory of semiconductor surfaces *Phys. Rev.* **99** 376–87

[3] Moss T S 1955 Photovoltaic and photoconductive theory applied to InSb *J. Electron. Control* **1** 126–38

[4] Brattain W H and Garrett C G B 1956 Combined measurements of field-effect, surface photo-voltage and photoconductivity *Bell Syst. Tech. J.* **35** 1019–40

[5] Morrison S R 1953 Changes of surface conductivity of germanium with ambient *J. Phys. Chem.* **57** 860–3

[6] Johnson E O 1957 Measurement of minority carrier lifetime with the surface photovoltage *J. Appl. Phys.* **28** 1349–53

[7] Quilliet A and Gosar P 1960 The surface photovoltaic effect in silicon and its application to measure the minority carrier lifetime *J. Physique Radium* **21** 575–80 (in French)

[8] Goodman A M 1961 A method for the measurement of short minority carrier diffusion lengths in semiconductors *J. Appl. Phys.* **32** 2550–2

[9] Goodman A M, Goodman L A and Gossenberger H F 1983 Silicon-wafer process evaluation using minority-carrier diffusion length measurements by the SPV method *RCA Rev.* **44** 326–41

[10] Nakhmanson R S 1975 Frequency dependence of the photo-EMF of strongly inverted Ge and Si MIS structures—I. Theory *Solid-State Electron.* **18** 617–26
Nakhmanson R S 1975 Frequency dependence of the photo-EMF of strongly inverted Ge and Si MIS structures—II. Experiment *Solid-State Electron.* **18** 627–34

[11] Lehovec K and Slobodskoy A 1964 Impedance of semiconductor–insulator–metal capacitors *Solid-State Electron.* **7** 59–79

[12] Hofstein S R and Warfield G 1965 Physical limitations on the frequency response of a semiconductor surface inversion layer *Solid-State Electron.* **8** 321–41

[13] Lord Kelvin 1881 On a method of measuring contact electricity *Nature* April 1881
Lord Kelvin 1898 Contact electricity of metals *Phil. Mag.* **46** 82–121

[14] Kronik L and Shapira Y 1999 Surface photovoltage phenomena: theory, experiment, and applications *Surf. Sci. Rep.* **37** 1–206

[15] Johnson E O 1958 Large-signal surface photovoltage studies with germanium *Phys. Rev.* **111** 153–66

[16] Semiconductor Diagnostics, Inc. 1993 *Contamination Monitoring System Based on SPV Diffusion Length Measurements* Manual SDI

[17] Shaffert R M 1975 *Electrophotography* (New York: Wiley)

[18] Williams R and Willis A 1968 Electron multiplication and surface charge on zinc oxide single crystals *J. Appl. Phys.* **39** 3731–6

[19] Williams R and Woods M H 1973 High electric fields in silicon dioxide produced by corona charging *J. Appl. Phys.* **44** 1026–8

[20] Weinberg Z A 1977 Tunneling of electrons from Si into thermally grown SiO_2 *Solid-State Electron.* **20** 11–18

[21] Woods M H and Williams R 1973 Injection and removal of ionic charge at room temperature through the interface of air with SiO_2 *J. Appl. Phys.* **44** 5506–10

[22] Comizzoli R B 1987 Uses of corona discharges in the semiconductor industry *J. Electrochem. Soc.* **134** 424–9

[23] Schroder D K, Fung M S, Verkuil R L, Pandey S, Howland W H and Kleefstra M 1998 Corona-oxide-semiconductor device characterization *Solid-State Electron.* **42** 505–12

[24] Lagowski J and Edelman P 1997 Contact potential difference methods for full wafer characterization of oxidized silicon *7th Int. Conf. on Defect Recognition and Image Processing (1997)*

[25] Pierret R F 1996 *Semiconductor Device Fundamentals* (Reading, MA: Addison-Wesley)

[26] Johnson E O 1958 Large-signal surface photovoltage studies with germanium *Phys. Rev.* **111** 153–66

[27] Choo S C and Mazur R G 1970 Open circuit voltage behavior of junction devices *Solid-State Electron.* **13** 553–64

[28] Moore A R 1983 Theory and experiment on the surface-photovoltage diffusion-length measurement as applied to amorphous silicon *J. Appl. Phys.* **54** 222–8
Chiang C L, Schwarz R, Slobodin D E, Kolodzey J and Wagner S 1986 Measurement of the minority-carrier diffusion length in thin semiconductor films *IEEE Trans. Electron Devices* **33** 1587–92
Chiang C L and Wagner S 1985 On the theoretical basis of the surface photovoltage technique *IEEE Trans. Electron Devices* **32** 1722–6

[29] Schroder D K 1997 Carrier lifetimes in silicon *IEEE Trans. Electron Devices* **44** 160–70

[30] Lagowski J, Edelman P, Dexter M and Henley W 1982 Non-contact mapping of heavy metal contamination for silicon IC fabrication *Semicond. Sci. Technol.* **7** A185–92

[31] Michel J, Reddy A J, Norga G F, Platero M and Kimerling L C 1997 *In-situ* determination of Si wafer contamination using photoconductance decay measurements *Diagnostic Techniques for Semiconductor Materials and Devices* PV97-12, ed P Rai-Choudhury *et al* (Princeton, NJ: Electrochemical Society) pp 212–22

[32] Mishra K and Falster R 1992 *Electrochem. Soc. Meeting Extended Abstracts* 92-2 *(Toronto, 1992)* Abstract 426, p 632

[33] Lagowski J, Edelman P, Kontkiewicz A M, Milic O, Henley W, Jastrzebski L and Hoff A M 1993 Iron detection in the part per quadrillion range in silicon using surface photovoltage and photodissociation of iron–boron pairs *Appl. Phys. Lett.* **32** 3043–5

[34] Zoth G and Bergholz W 1990 A fast, preparation-free method to detect iron in silicon *J. Appl. Phys.* **67** 6764–71

[35] Zoth G and Bergholz W 1990 A fast, preparation-free method to detect iron in silicon *J. Appl. Phys.* **67** 6764–71
Antilla O J and Tilli M V 1992 Metal contamination removal on silicon wafers using dilute acidic solutions *J. Electrochem. Soc.* **139** 1751–6
Kitagawara Y, Yoshida T, Hamaguchi T and Takenaka T 1995 Evaluation of oxygen-related carrier recombination centers in high-purity Czochralski-grown Si crystals by the bulk lifetime measurements *J. Electrochem. Soc.* **142** 3505–9

Miyazaki M, Miyazaki S, Kitamura T, Aoki T, Nakashima Y, Hourai M and Shigematsu T 1995 Influence of Fe contamination in Czochralski-grown silicon single crystals on LSI-yield related crystal quality characteristics *Japan. J. Appl. Phys.* **34** 409–13

Rotondaro A L P, Hurd T Q, Kaniava A, Vanhellemont J, Simoen E, Heyns M M and Claeys C 1996 Impact of Cu and Fe contamination on the minority carrier lifetime of silicon substrates *J. Electrochem. Soc.* **143** 3014–19

[36] Henley W, Ramappa D and Jastrzebski L 1999 Detection of copper contamination in silicon by surface photovoltage diffusion length measurements *Appl. Phys. Lett.* **74** 278–80

[37] Schroder D K 1998 *Semiconductor Material and Device Characterization* 2nd edn (New York: Wiley–Interscience) pp 459–63

[38] Renaud P and Walker A 2000 Measurement of carrier lifetime: monitoring epitaxy quality *Solid State Technol.* **43** 143–6

[39] DeBusk D K and Hoff A M 1999 Fast noncontact diffusion-process monitoring *Solid State Technol.* **42** 67–74

[40] Weinzierl S R and Miller T G 1999 Non-contact corona-based process control measurements: where we've been and where we're headed *Analytical and Diagnostic Techniques for Semiconductor Materials, Devices, and Processes* ECS 99-16, ed B O Kolbesen *et al* (Princeton, NJ: Electrochemical Society) pp 342–50

[41] Nauka K and Lagowski J 1998 Advances in surface photovoltage techniques for monitoring of the IC processes *Characterization and Metrology for ULSI Technology: 1998 Int. Conf.* ed D G Seiler *et al* (American Institute of Physics) pp 245–9

Fung M S 1997 Monitoring PSG plasma damage with COS *Semicond. Int.* **20** 211–18

[42] Nauka K 1997 Contactless measurement of the Si–buried oxide interfacial charges in SOI wafers with surface photovoltage technique *Microelectron. Eng.* **36** 351–7

[43] Roy P K, Chacon C, Ma Y, Kizilyalli I C, Horner G S, Verkuil R L and Miller T G 1997 Non-contact characterization of ultrathin dielectrics for the gigabit era *Diagnostic Techniques for Semiconductor Materials and Devices* PV97-12, ed P Rai-Choudhury *et al* (Princeton, NJ: Electrochemical Society) pp 280–94

[44] Miller T G 1995 A new approach for measuring oxide thickness *Semicond. Int.* **18** 147–8

[45] Lo S H, Buchanan D A and Taur Y 1999 Modeling and characterization of quantization, polysilicon depletion, and direct tunneling effects in MOSFETs with ultrathin oxides *IBM J. Res. Dev.* **43** 327–37

[46] Weinberg Z A, Johnson W C and Lampert M A 1976 High-field transport in SiO_2 on silicon induced by corona charging of the unmetallized surface *J. Appl. Phys.* **47** 248–55

[47] Munakata C, Nishimatsu S, Homma N and Yagi K 1984 AC surface photovoltages in strongly-inverted oxidized p-type silicon wafers *Japan. J. Appl. Phys.* **11** 1451–61

Munakata C and Nishimatsu S 1986 Analysis of ac surface photovoltages in a depleted oxidized p-type silicon wafer *Japan. J. Appl. Phys.* **25** 807–12

[48] Kinameri K, Munakata C and Mayama K 1988 A scanning photon microscope for non-destructive observations of crystal defect and interface trap distributions in silicon wafers *J. Phys. E: Sci. Instrum.* **21** 91–7

[49] Shimizu H and Munakata C 1993 Nondestructive diagnostic method using ac surface photovoltage for detecting metallic contaminants in silicon wafers *J. Appl. Phys.* **73** 8336–9

[50] Kamieniecki E 1998 Non-contact measurements of the minority carrier recombination lifetime at the silicon surface *Recombination Lifetime Measurements in Silicon* ASTM, STP 1340, ed D C Gupta, F R Bacher and W M Hughes, pp 147–55

[51] Liberman S 1998 Surface minority carrier lifetime measurements using modulated photocurrent *Recombination Lifetime Measurements in Silicon* ASTM, STP 1340, ed D C Gupta, F R Bacher and W M Hughes, pp 156–67

[52] Roman P, Staffa J, Fakhouri S, Brubaker M, Ruzyllo J, Torek K and Kamieniecki E 1998 Surface dopant concentration monitoring using noncontact surface charge profiling *J. Appl. Phys.* **83** 2297–300

[53] Nguyen M C, Tower J P and Danel A 1999 Epilayer quality and yield improvement using the surface charge profiler as a non-destructive diagnostic technique *Analytical and Diagnostic Techniques for Semiconductor Materials, Devices, and Processes* ECS 99-16, ed B O Kolbesen *et al* (Princeton, NJ: Electrochemical Society) pp 408–18

[54] Green M A and Keevers M J 1995 Optical properties of intrinsic silicon at 300 K *Prog. Photovolt.* **3** 189–92

[55] ASTM Standard F391-96 1996 Standard test method for minority-carrier diffusion length in silicon by measurement of steady-state surface photovoltage *1996 Annual Book of ASTM Standards* (West Conshohocken, PA: American Society for Testing of Materials)

[56] Phillips W E 1972 Interpretation of steady-state surface photovoltage measurements in epitaxial semiconductor layers *Solid-State Electron.* **15** 1097–102

[57] Antilla O J and Hahn S K 1993 Study on surface photovoltage measurement of long diffusion length silicon: simulation results *J. Appl. Phys.* **74** 558–69

[58] Hara T, Tamura F and Kitamura T 1997 Minority carrier lifetime measurements in epitaxial silicon layers *J. Electrochem. Soc.* **144** L54–7

[59] Lagowski J, Faifer V and Edelman P 1996 Recent refinements in the surface photovoltage method for measuring very long minority carrier diffusion length *Proc. Electrochem. Soc.* **96-13** 512–22

[60] Lagowski J, Edelman P and Faifer V 1998 Present status of the surface photovoltage method (SPV) for measuring minority carrier diffusion length and related parameters *Recombination Lifetime Measurements in Silicon* ASTM, STP 1340, ed D C Gupta, F R Bacher and W M Hughes, pp 125–44

[61] Zoth G, Geyer S and Schulze H J 1999 Silicon contamination control by lifetime measurements *Analytical and Diagnostic Techniques for Semiconductor Materials, Devices, and Processes* ECS 99-16, ed B O Kolbesen *et al* (Princeton, NJ: Electrochemical Society) pp 5–20

[62] Schroder D K 1998 *Semiconductor Material and Device Characterization* 2nd edn (New York: Wiley-Interscience) pp 485–7